Korean J. Chem. Eng., 34(12), 3085-3091 (2017)
DOI: 10.1007/s11814-017-0257-0

pISSN: 0256-1115
eISSN: 1975-7220

CO and CO_2 methanation over Ni catalysts supported on alumina with different crystalline phases

Thien An Le, Tae Wook Kim, Sae Ha Lee, and Eun Duck Park†

Department of Chemical Engineering and Department of Energy Systems Research, Ajou University, Suwon 16499, Korea
(*Received 8 August 2017 • accepted 18 September 2017*)

Abstract−The effect of alumina crystalline phases on CO and CO_2 methanation was investigated using alumina-supported Ni catalysts. Various crystalline phases, such as α-Al_2O_3, θ-Al_2O_3, δ-Al_2O_3, η-Al_2O_3, γ-Al_2O_3, and κ-Al_2O_3, were utilized to prepare alumina-supported Ni catalysts via wet impregnation. N_2 physisorption, H_2 chemisorption, temperature-programmed reduction with H_2, CO_2 chemisorption, temperature-programmed desorption of CO_2, and X-ray diffraction were employed to characterize the catalysts. The Ni/θ-Al_2O_3 catalyst showed the highest activity during both CO and CO_2 methanation at low temperatures. CO methanation catalytic activity appeared to be related to the number of Ni surface-active sites, as determined by H_2-chemisorption. During CO_2 methanation, Ni dispersion and the CO_2 adsorption site were found to influence catalytic activity. Selective CO methanation in the presence of excess CO_2 was performed over Ni/γ-Al_2O_3 and Ni/δ-Al_2O_3; these substrates proved more active for CO methanation than for CO_2 methanation.

Keywords: CO Methanation, CO_2 Methanation, Ni/Al_2O_3, Alumina, Crystalline Phase

INTRODUCTION

CO methanation ($CO+3H_2 \leftrightarrow CH_4+H_2O$) is one of the chemical reactions used to convert synthesis gas, which is a mixture of CO and H_2 produced through gasification of a variety of feedstocks such as biomass, coal, and organic waste [1]. Recently, CO_2 methanation ($CO_2+4H_2 \leftrightarrow CH_4+2H_2O$) has also gained attention as an option for transforming CO_2, a major greenhouse gas, into valuable chemicals using hydrogen generated with renewable energy [2]. Separately, selective CO methanation in the presence of CO_2 has been proposed to remove residual CO in the fuel processor hydrogen stream in polymer electrolyte membrane fuel cells (PEMFCs), as the electrochemical performance of the Pt anode in PEMFCs deteriorates in the presence of even trace amounts of CO [3].

These CO and CO_2 methanation methods, called Sabatier reactions [4], are the focus of numerous studies exploring the development of catalysts and related processes [1,5-8]. Although catalytic activity during CO methanation decreases for common catalysts in the following order: Ru>Fe>Ni>Co>Rh>Pd>Pt and Ir [9], Ni-based catalysts have been widely used in commercial processes because of their fair activity, low cost, and high availability compared to noble-metal catalysts.

Catalytic activities for CO and CO_2 methanation over supported Ni catalysts are strongly dependent on the nature of the support [10,11]. Alumina is one of the most commonly employed industrial support materials due to its high thermal stability and strong resistance to attrition [12]. Various crystalline phases of alumina can be synthesized from a number of precursors under different thermal conditions [13-15]. Each phase of alumina has different physicochemical properties resulting in different catalytic activity [16-20]. In the case of γ-Al_2O_3, the surface defect site can stabilize small metal clusters to suppress metal particle aggregation during the catalytic reaction [18,19]. On the other hand, strong interactions between metal oxides and the γ-Al_2O_3 surface defect site often hinder reduction of the metal oxide and inhibit the formation of active metals [20]. Therefore, we might expect that interactions between NiO and alumina surface sites will vary with different crystalline phases. However, to the best of our knowledge, no previous studies have explored the effect of alumina crystalline phase on CO and CO_2 methanation using Ni catalysts.

In this study, we prepared alumina supports with different crystalline phases including α-Al_2O_3, θ-Al_2O_3, δ-Al_2O_3, η-Al_2O_3, γ-Al_2O_3, and κ-Al_2O_3. The alumina-supported Ni catalysts were synthesized using a wet impregnation method; these catalysts were applied during CO and CO_2 methanation. We found that the interaction between NiO and the alumina surface site varies according to the alumina crystalline phase, and that Ni/θ-Al_2O_3 displays the highest catalytic activity during both CO and CO_2 methanation. Additionally, Ni/γ-Al_2O_3 and Ni/δ-Al_2O_3 catalysts are promising candidates for selective CO methanation in the presence of CO_2, as these catalysts are more active for CO methanation than for CO_2 methanation.

EXPERIMENTAL

1. Catalyst Preparation

Different crystalline phases of alumina were synthesized from various alumina precursors such as bayerite, gibbsite, and boehmite through the thermal decomposition as described in the previous work [18]. The detailed procedure is depicted in the supporting information. α-Al_2O_3 (Kanto Chem.) was purchased and utilized

†To whom correspondence should be addressed.
E-mail: edpark@ajou.ac.kr

as delivered.

Ni/Al_2O_3 catalysts were prepared from an aqueous $Ni(NO_3)_2$ solution and alumina support using a wet impregnation method as described in detail in the supporting information.

2. Catalyst Characterization

The surface area of the sample was calculated with the Brunauer-Emmett-Teller (BET) method based on the N_2 physisorption data. The primary crystallite size of the metallic Ni in each catalyst was calculated using the Scherrer equation [21] based on the powder X-ray diffraction (XRD) data. The reducibility of Ni oxide species, Ni content, and reduction degree of Ni oxide species for each catalyst were probed using hydrogen temperature-programmed reduction (H_2-TPR). The amount of CO_2 chemisorbed at room temperature and adsorption strength of CO_2 on the catalyst was investigated with pulsed CO_2 chemisorption and temperature-programmed desorption of CO_2 (CO_2-TPD), respectively. H_2 chemisorption was also performed to determine the catalytic active surface area (CASA) of the catalyst assuming that one hydrogen atom resides on one surface Ni atom and that the cross-sectional area of the Ni atom is 6.49×10^{-20} m^2 [22]. The detailed procedure for each characterization technique is described in the supporting information.

3. Catalytic Activity Tests

CO and CO_2 methanation were performed in a fixed-bed reactor with an internal diameter of 3 mm and length of 345 mm. The flow rate of each gas was controlled with a mass flow controller (MFC; Brooks Instruments). The reaction temperature was monitored with a thermocouple located in the catalyst bed. The catalysts, which were retained between 45 and 80 mesh sieves, were reduced in situ at 600 °C in an H_2 stream with a flow rate of 30 mL/min for 1 h before each reaction. The catalytic activity was measured at atmospheric pressure at the reaction temperature, which ranged from 150 to 400 °C. The feed gas, which was composed of 1 mol% CO (or CO_2), 50 mol% H_2, and 49 mol% He, contacted 0.10 g of the catalyst at a flow rate of 100 mL/min. The kinetic experiments, which were performed separately under different reaction conditions, featured 0.10 g of a given catalyst diluted with 0.20 g of α-alumina in contact with the feed gas described above. CO and CO_2 conversions were controlled to achieve less than 15%. The activation energy (Ea) over each catalyst was calculated based on the Arrhenius equation:

$$k = A\exp\left(-\frac{Ea}{RT}\right) \quad (1)$$

where k denotes the reaction rate constant, A is the frequency factor, Ea is the activation energy, R is the gas constant, and T is the absolute temperature.

Selective CO methanation in the presence of CO_2 was studied at atmospheric pressure in the same reactor. The typical feed composition was 0.3 (or 1.0) mol% CO, 20 mol% CO_2, 50 mol% H_2, and 29.7 (or 29) mol% He.

The outlet gas compositions were analyzed online using a gas chromatograph (YL Instrument 6100GC), which was equipped with either a packed column filled with Carbosphere® for TCD or a capillary Poralot Q column for flame ionization detection (FID). CO conversion (X_{CO}), CO_2 conversion (X_{CO_2}), CO yield (Y_{CO}), and C_1-C_3 hydrocarbon yield ($Y_{C_xH_y}$) were calculated using the following equations:

$$X_{CO_z}(\%) = \frac{(CO_z)_{in} - (CO_z)_{out}}{(CO_z)_{in}} \times 100 \quad (2)$$

$$Y_{CO}(\%) = \frac{(CO)_{out}}{(CO_2)_{in}} \times 100 \quad (3)$$

$$Y_{C_xH_y}(\%) = \frac{x(C_xH_y)_{out}}{(CO)_{in} + (CO_2)_{in}} \times 100 \quad (4)$$

where $(CO_z)_{in}$, $(CO_z)_{out}$, and $(C_xH_y)_{out}$ represent the molar flow rate of CO_z entering the reactor, the molar flow rate of CO_z out of the reactor, and the molar flow rate of C_xH_y exiting the reactor, respectively.

RESULTS AND DISCUSSION

1. Physicochemical Properties of the Catalysts

The N_2 physisorption data for alumina supports with different crystalline phases show that the specific surface area of the supports decreases as follows: η-Al_2O_3>γ-Al_2O_3>θ-Al_2O_3, δ-Al_2O_3>κ-Al_2O_3>α-Al_2O_3 (Table S1). The average pore diameter of these

Table 1. Physicochemical properties of Ni/Al_2O_3 catalysts

Catalyst	Ni content[a] (wt%)	Specific surface area (m^2/g)	Pore volume (cm^3/g)	Average pore diameter[b] (nm)	Degree of reduction[c] (%)	CO_2 uptake[d] (μmol/g)	CASA[e] ($m^2/g_{cat.}$)	Ni crystallite size[f] (nm)
Ni/θ-Al_2O_3	10	76	0.26	14	91	24	3.3	-
Ni/δ-Al_2O_3	9	67	0.21	13	100	19	2.1	8
Ni/η-Al_2O_3	10	139	0.23	7	55	37	2.5	-
Ni/γ-Al_2O_3	10	94	0.22	9	88	14	2.3	7
Ni/κ-Al_2O_3	9	18	0.14	31	100	12	1.3	16
Ni/α-Al_2O_3	10	<1	-	-	100	0.2	0.3	33

[a]Ni content was determined using inductively coupled plasma-atomic emission spectroscopy (ICP-AES)

[b]Average pore diameter were determined using a BJH model

[c]Degree of reduction of reduced catalysts at 600 °C was measured by H_2-TPR

[d]CO_2 uptake was determined based on CO_2 chemisorption

[e]Catalytic active surface area (CASA) was determined based on H_2 chemisorption

[f]Ni crystallite size was calculated using the Scherrer formula with XRD data

supports decreases in the following order: κ-Al_2O_3>θ-Al_2O_3>δ-Al_2O_3>γ-Al_2O_3>η-Al_2O_3 (Table S1). N_2 physisorption data for Ni catalysts supported by alumina with different crystalline phases are listed in Table 1. The specific surface area and pore volume for Ni-treated supports were decreased somewhat compared with those of the given support by itself, with the exception of Ni/κ-Al_2O_3; this implies that the nickel precursor was homogeneously impregnated into the inner pore walls of the alumina support. N_2 adsorption-desorption isotherms and pore size distributions for all catalysts are displayed in Fig. S1. All the catalysts except for Ni/α-Al_2O_3 display H_2 hysteresis during the adsorption and desorption processes, indicating the presence of disordered pores. In the case of Ni/α-Al_2O_3, there were no noticeable peaks corresponding to micro- or mesopores in the pore size distribution obtained from the N_2 desorption isotherm.

X-ray diffraction patterns were obtained for the alumina supports and Ni/Al_2O_3 catalysts, and are displayed in Fig. S2 and Fig. 1, respectively. The presence of single-phase alumina can be confirmed, as each support has its own characteristic bulk crystalline structure (Fig. S2). For all reduced Ni/Al_2O_3 catalysts, the Ni metal phase (JCPDS No. 04-0850) was observed at 2θ=44.5, 51.8, and 76.3°, as shown in Fig. 1. The crystallite size of Ni was calculated using the Scherrer equation and is listed in Table 1. The crystallite sizes of Ni were determined to be 7, 8, 16, and 33 nm for Ni/γ-Al_2O_3, Ni/δ-Al_2O_3, Ni/κ-Al_2O_3, and Ni/α-Al_2O_3, respectively. For both Ni/θ-Al_2O_3 and Ni/η-Al_2O_3, the crystallite size of Ni cannot be calculated using the Scherrer equation because the major Ni and support XRD peaks overlap. It is worth mentioning that the crystallite size of Ni is inversely proportional to the specific surface area of the support; the largest Ni crystallite size was obtained for Ni/α-Al_2O_3, which also has the smallest surface area.

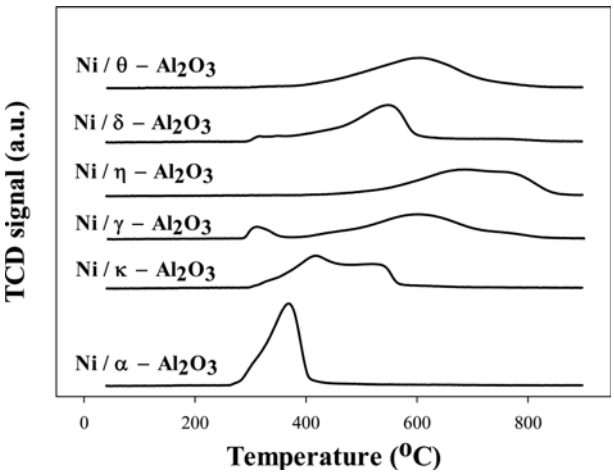

Fig. 2. H_2-TPR profiles for Ni/Al_2O_3 catalysts calcined at 500 °C.

H_2-TPR patterns were obtained for Ni/Al_2O_3 catalysts calcined at 500 °C (Fig. 2). The low-temperature TPR peak observed for Ni/γ-Al_2O_3, Ni/δ-Al_2O_3, and Ni/α-Al_2O_3 in the 310-400 °C temperature range is due to the reduction of NiO interacting weakly with a support [23,24]. On the other hand, the TPR peak in the 400-600 °C temperature range is ascribed to the reduction of NiO interacting strongly with a support [23,24]. For Ni/Al_2O_3 catalysts, $NiAl_2O_4$ may be formed during the calcination step and reduced at temperatures above 600 °C [23,24]. In this study, the presence of $NiAl_2O_4$

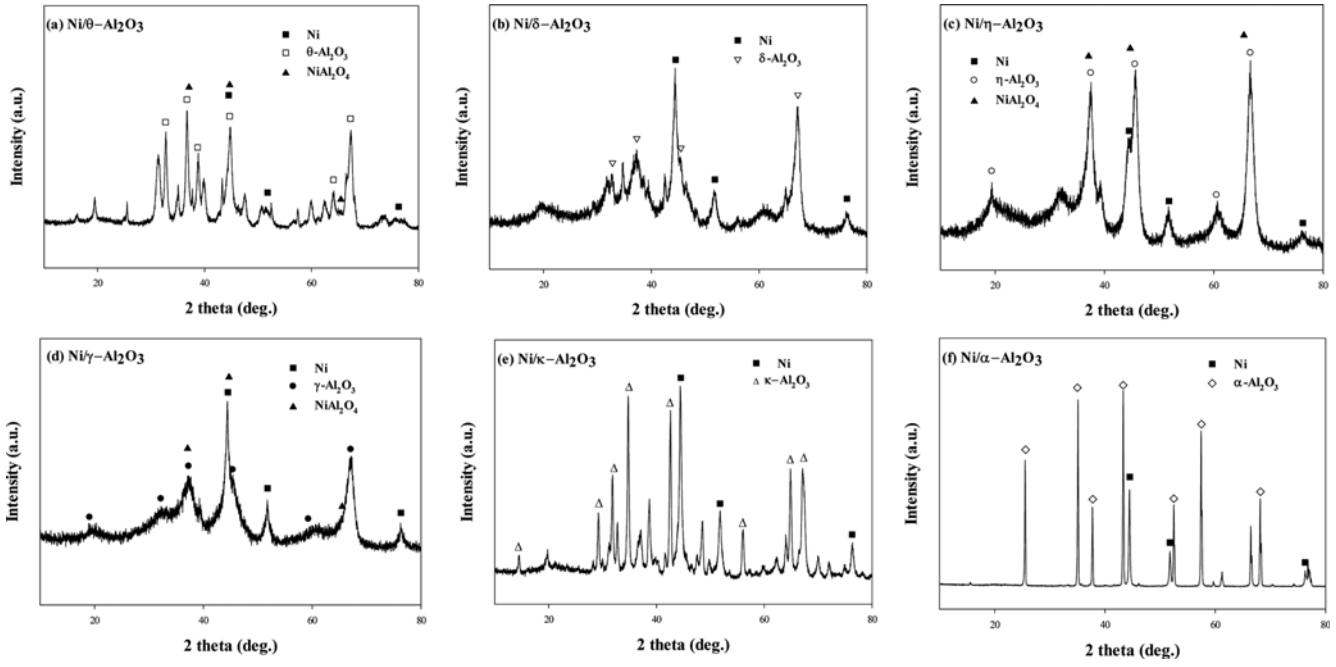

Fig. 1. X-ray diffraction patterns for Ni/Al_2O_3 catalysts reduced at 600 °C. (a) Ni/θ-Al_2O_3, (b) Ni/δ-Al_2O_3, (c) Ni/η-Al_2O_3, (d) Ni/γ-Al_2O_3, (e) Ni/κ-Al_2O_3, and (f) Ni/α-Al_2O_3. (□) θ-Al_2O_3 (JCPDS 35-0121), (▽) δ-Al_2O_3 (JCPDS 88-1609), (○) η-Al_2O_3 (JCPDS 04-0875), (●) γ-Al_2O_3 (JCPDS 29-0063), (△) κ-Al_2O_3 (JCPDS 88-0107), (◇) α-Al_2O_3 (JCPDS 42-1468), (■) Ni (JCPDS 04-0850), (▲) $NiAl_2O_4$ (JCPDS 10-0339).

was confirmed in XRD data for Ni/γ-Al_2O_3, Ni/θ-Al_2O_3, and Ni/η-Al_2O_3 (Fig. 1); these catalysts also have a high-temperature TPR peak. Most Ni oxide species in Ni/δ-Al_2O_3, Ni/κ-Al_2O_3, and Ni/α-Al_2O_3 appear to be transformed into the metallic state when they are reduced at 600 °C. However, the high-temperature TPR peak was observed above 600 °C for Ni/γ-Al_2O_3, Ni/θ-Al_2O_3, and Ni/η-Al_2O_3. Since all the catalysts were reduced at 600 °C in this study, the degree of reduction for each catalyst was calculated and listed in Table 1. Complete reduction of nickel oxide was achieved in the Ni/δ-Al_2O_3, Ni/κ-Al_2O_3, and Ni/α-Al_2O_3 catalysts. However, only partial reduction of the nickel oxide species was realized in the Ni/γ-Al_2O_3, Ni/θ-Al_2O_3, and Ni/η-Al_2O_3 catalysts. Remarkably, only one-half of the nickel oxide species in Ni/η-Al_2O_3 were reduced at 600 °C.

To determine the metallic surface area of Ni in Ni/Al_2O_3 catalysts reduced at 600 °C, the H_2 chemisorption was carried out and its results are listed in Table 1. The CASA decreased in the following order: Ni/θ-Al_2O_3>Ni/η-Al_2O_3>Ni/γ-Al_2O_3>Ni/δ-Al_2O_3>Ni/κ-Al_2O_3>Ni/α-Al_2O_3. The CASA is inversely related to the Ni crystallite size (as determined by XRD data), which is reasonable because smaller metal particles provide higher metal surface areas. However, the CASA does not appear to be directly related to the degree of reduction. The number of large NiO particles interacting weakly with a support may be reduced at low temperatures, resulting in a high degree of reduction. Therefore, a high degree of reduction does not guarantee high CASA because large Ni particles may be formed from large NiO particles. The smallest CASA was obtained for Ni/α-Al_2O_3, which also features complete reduction and the largest Ni crystallite sizes.

CO_2 chemisorption was performed to determine the number of surface basic sites on Ni/Al_2O_3 catalysts; the results are listed in Table 1. The amount of chemisorbed CO_2 was determined to be 37, 24, 19, 14, 12, and 0.2 μmol/g for Ni/η-Al_2O_3, Ni/θ-Al_2O_3, Ni/δ-Al_2O_3, Ni/γ-Al_2O_3, Ni/κ-Al_2O_3, and Ni/α-Al_2O_3, respectively. The amount of chemisorbed CO_2 appears to be related to the specific surface area of the catalyst only except for Ni/γ-Al_2O_3. In the previous FT-IR studies, the presence of bicarbonates produced via the interaction of CO_2 with the basic surface hydroxyl groups on the alumina surface was confirmed [25]. Since these carbonate species are reported to be formed in the presence of relatively more basic O sites, such as surface O^{2-} sites, rather than on O atoms related to conventional surface hydroxyl groups [25,26], an exact linear correlation cannot be made between the specific surface area and the amount of chemisorbed CO_2 at room temperature.

CO_2-TPD patterns were used to monitor the strength of CO_2 adsorption onto each catalyst. As shown in Fig. 3, all of the catalysts except for Ni/κ-Al_2O_3 show a single TPD peak at ~100 °C. This TPD peak can be assigned to CO_2 which is weakly molecularly adsorbed on the catalyst surface [27]. For the Ni/κ-Al_2O_3 catalyst, a high-temperature shoulder peak was also observed beside the low-temperature TPD peak, implying that moderately basic sites are present along with weakly basic sites.

2. Catalyst Performance

2-1. CO Methanation

Catalytic performance during CO methanation was measured for Ni/Al_2O_3 catalysts with different alumina crystalline phases. As shown in Fig. 4(a), CO conversion at fixed temperature decreased for the various catalysts in the following order: Ni/θ-Al_2O_3>Ni/γ-

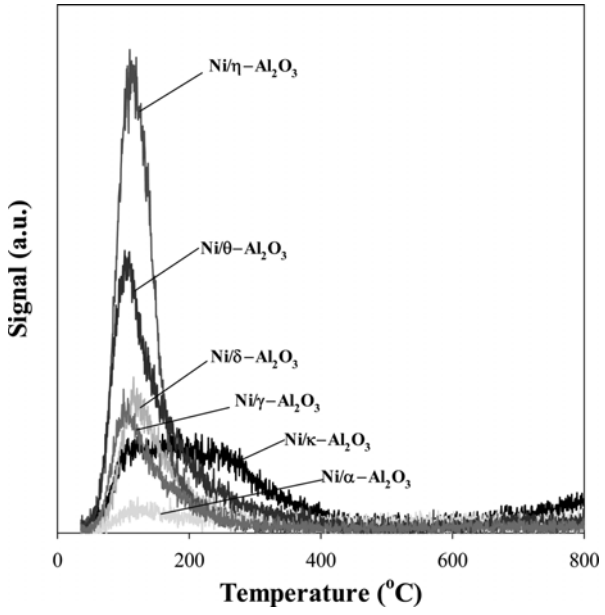

Fig. 3. CO_2-TPD profiles for Ni/Al_2O_3 catalysts reduced at 600 °C.

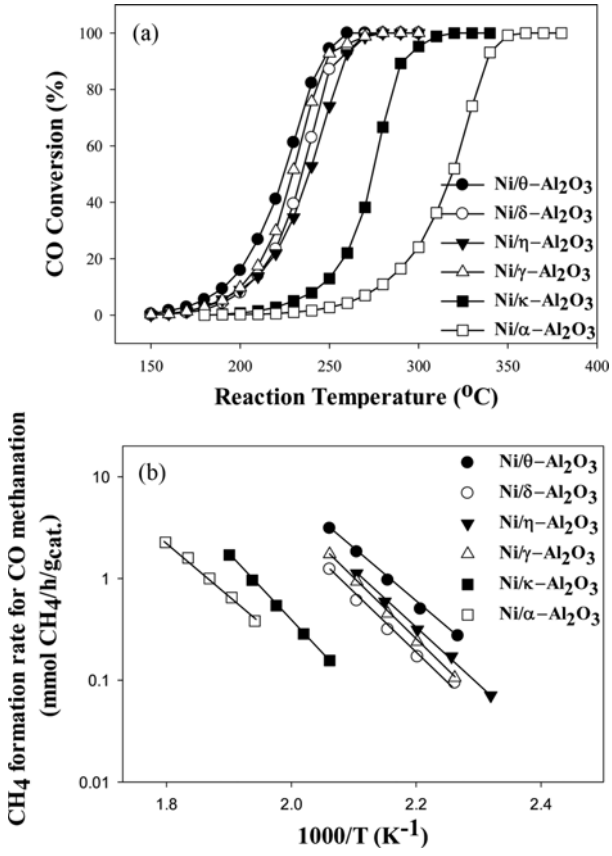

Fig. 4. (a) Catalytic performance of Ni/Al_2O_3 catalysts, and (b) formation rate of CH_4 for CO methanation. Reaction conditions: 1 mol% CO, 50 mol% H_2, 49 mol% He, F/W=1,000 mL/min/g_{cat}.

Al_2O_3>Ni/δ-Al_2O_3>Ni/η-Al_2O_3>Ni/κ-Al_2O_3>Ni/α-Al_2O_3. Among the catalysts tested, Ni/θ-Al_2O_3 and Ni/α-Al_2O_3 possessed the highest and lowest catalytic activity, respectively; Ni/θ-Al_2O_3 and Ni/α-Al_2O_3 also had the largest and smallest CASA, respectively. This is consistent with previous work showing that Ni particle size is critical for catalytic performance in CO methanation over supported Ni catalysts [28,29]. Methane, ethane, and propane were detected as major products of this reaction; the carbon yield to each product is displayed in Fig. S3. In all cases, methane was the predominant product at all reaction temperatures, regardless of the catalyst. The carbon yield for C_{2+} hydrocarbons increased with increasing CO conversion and decreased with further CO conversion after reaching a maximum at intermediate CO conversion. At temperatures at which 100% CO conversion was achieved, only methane was formed. The fixed-temperature carbon yield was decreased irrespective of the catalyst in the following order: methane>ethane>propane. Note that Ni/γ-Al_2O_3 and Ni/δ-Al_2O_3 produced much higher carbon yields for ethane and propane than did the other Ni/Al_2O_3 catalysts. Conversely, no propane formation was observed over either Ni/κ-Al_2O_3 or Ni/α-Al_2O_3. Fig. 4(b) shows an Arrhenius plot of the methane formation rates for various Ni/Al_2O_3 catalysts versus the reciprocal value of the absolute temperature for CO methanation. The apparent activation energy (Ea) values for the CO methanation methane formation rate were determined to be 108, 125, 115, 100, 134, and 118 kJ/mol for Ni/θ-Al_2O_3, Ni/γ-Al_2O_3, Ni/δ-Al_2O_3, Ni/η-Al_2O_3, Ni/κ-Al_2O_3, and Ni/α-Al_2O_3, respectively. These activation energies are comparable to those in previous studies; Bhatia et al. [30] found an activation energy of 110-122 kJ/mol for CO methanation over 11 wt% Ni/η-Al_2O_3 at temperatures spanning 235-295 °C, and Liu et al. [31] obtained an activation energy of 102 kJ/mol for CO methanation over 20 wt% Ni/α-Al_2O_3 at temperatures spanning 230-260 °C.

2-2. CO_2 Methanation

Catalytic performance during CO_2 methanation was obtained over Ni/Al_2O_3 catalysts as shown in Fig. 5(a). Fixed-temperature CO_2 conversion decreased among the catalysts in the following order: Ni/θ-Al_2O_3≈Ni/κ-Al_2O_3>Ni/η-Al_2O_3≈Ni/α-Al_2O_3>Ni/δ-Al_2O_3>Ni/γ-Al_2O_3. As observed for CO methanation, Ni/θ-Al_2O_3 had both the highest CASA and the best catalytic activity during CO_2 methanation. Interestingly, Ni/κ-Al_2O_3 exhibited CO_2 methanation catalytic activity comparable to that observed for Ni/θ-Al_2O_3; this can be explained by the fact that Ni/κ-Al_2O_3 has additional moderately basic sites for CO_2 chemisorption, as revealed by CO_2-TPD experiments. Pan et al. [27] proposed that moderately basic sites can promote the formation of monodentate formate species, thus enhancing CO_2 methanation activity. Methane and CO were major products during CO_2 methanation (Fig. S4). In any case, C_{2+} hydrocarbons were not detected over Ni/Al_2O_3 catalysts. During CO_2 methanation, CO can be produced via a reverse water-gas shift reaction ($CO_2+H_2 \leftrightarrow CO+H_2O$). CO formation was observed only over Ni/α-Al_2O_3, Ni/κ-Al_2O_3, and Ni/η-Al_2O_3. Note that noticeable CO carbon yield was also observed over Ni/α-Al_2O_3 and Ni/κ-Al_2O_3 with large Ni particles. The carbon yield for CO increased with increasing CO_2 conversion and decreased with the further CO_2 conversion after reaching a maximum at intermediate CO_2 conversion. At temperatures at which 100% CO_2 conversion was achieved, only methane was formed.

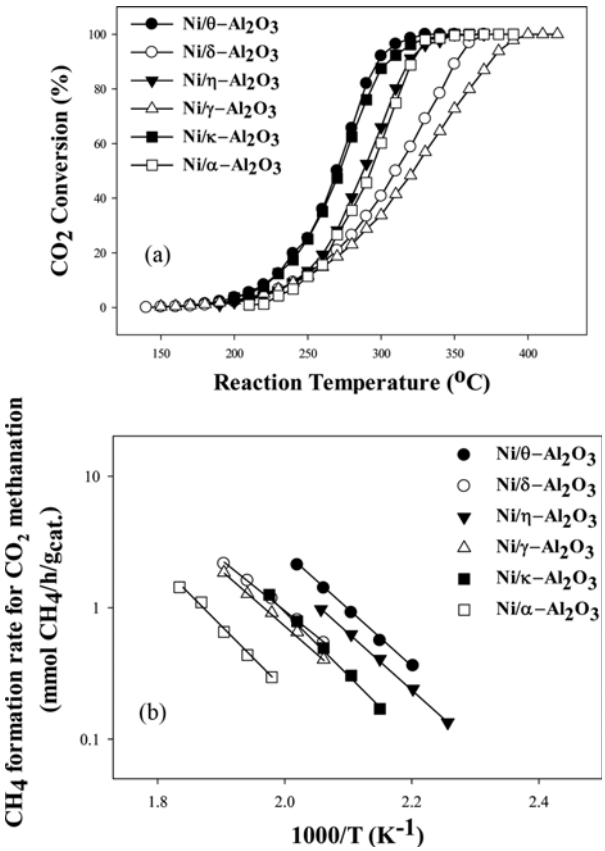

Fig. 5. (a) Catalytic performance, and (b) CH_4 formation rate for Ni/Al_2O_3 catalysts during CO_2 methanation. Reaction conditions: 1 mol% CO_2, 50 mol% H_2, 49 mol% He, F/W=1,000 mL/min/g_{cat}.

Fig. 5(b) shows an Arrhenius plot of methane formation rates for Ni/Al_2O_3 catalysts versus the reciprocal value of the absolute temperature for CO_2 methanation. The apparent activation energy (Ea) values for the methane formation rate during CO_2 methanation were 91, 91, 96, 101, 81, and 98 kJ/mol for Ni/θ-Al_2O_3, Ni/η-Al_2O_3, Ni/γ-Al_2O_3, Ni/κ-Al_2O_3, Ni/δ-Al_2O_3, and Ni/α-Al_2O_3, respectively. Ni/κ-Al_2O_3 had the highest activation energy for the methane formation rate during CO_2 methanation among the catalysts tested; this can explain the fact that Ni/κ-Al_2O_3 exhibits an activity comparable to that of Ni/θ-Al_2O_3 at high temperatures (Fig. 5(a)) even though Ni/κ-Al_2O_3 possesses a lower methane formation rate at low temperatures (Fig. 5(b)). The measured activation energies are comparable to those in previous studies; Herwijnen et al. [32] reported an activation energy of 106 kJ/mol for CO_2 methanation over 33.6 wt% Ni/Al_2O_3 at temperatures of 200-230 °C, while Garbarino et al. [33] obtained an activation energy of 80 kJ/mol for CO_2 methanation over 20 wt% Ni/Al_2O_3 at temperatures of 220-300 °C.

2-3. Selective CO Methanation

Because Ni/δ-Al_2O_3 and Ni/γ-Al_2O_3 were more active during CO methanation but less active during CO_2 methanation compared with the other Ni/Al_2O_3 catalysts, these catalysts were applied during selective CO methanation in the presence of excess CO_2. Ni/θ-

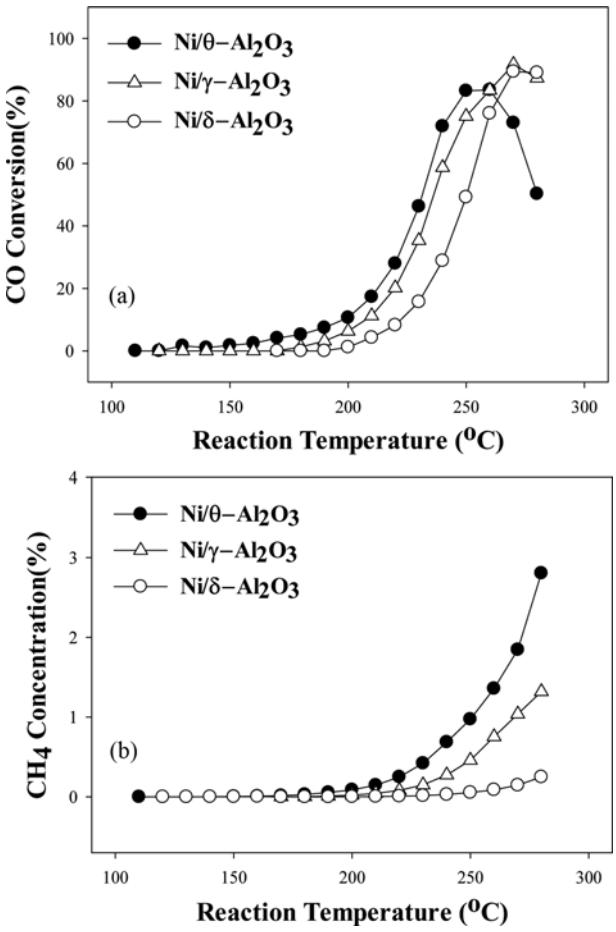

Fig. 6. (a) Catalytic performance of Ni/Al_2O_3 catalysts, and (b) CH_4 concentration in the exit stream during selective CO methanation. Reaction conditions: 1 mol% CO, 20 mol% CO_2, 50 mol% H_2, 29 mol% He, F/W=1,000 mL/min/g_{cat}.

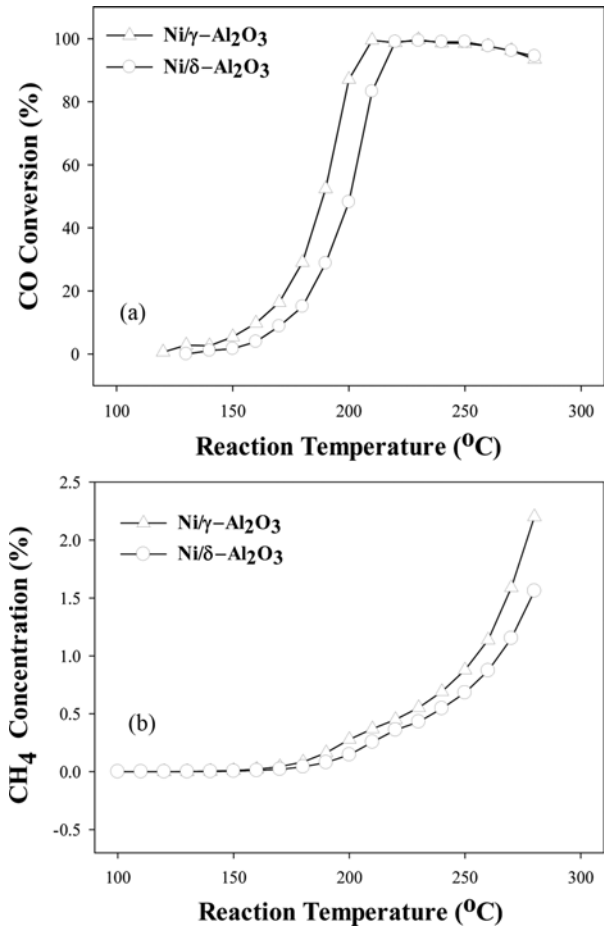

Fig. 7. (a) Catalytic performance of Ni/Al_2O_3 catalysts, and (b) CH_4 concentration in the exit stream during selective CO methanation. Reaction conditions: 0.3 mol% CO, 20 mol% CO_2, 50 mol% H_2, 29.7 mol% He, F/W=333 mL/min/g_{cat}.

Al_2O_3, which was the best catalyst for both CO and CO_2 methanation, was also tested for comparison. As shown in Fig. 6, CO conversion for all catalysts increased with increasing reaction temperature and decreased with further reaction temperature increases after reaching a maximum at an intermediate temperature. This decreasing CO conversion at high reaction temperatures is caused by the reverse water-gas shift reaction. CO conversions above 90% were not obtained over Ni/θ-Al_2O_3 despite the fact that this catalyst showed the highest methanation activity at low temperatures among the catalysts tested. Ni/γ-Al_2O_3 and Ni/δ-Al_2O_3 exhibited CO conversions around 90%, with Ni/γ-Al_2O_3 exhibiting higher methanation activity than Ni/δ-Al_2O_3. In all cases, the CH_4 concentration in the exit stream increased with reaction temperature. At high temperatures, concentrations of CH_4 in the exit stream were higher than CO concentrations in the inlet stream over Ni/θ-Al_2O_3 and Ni/γ-Al_2O_3, which implies that CO_2 was also transformed into CH_4.

Selective CO methanation was also performed over the Ni/δ-Al_2O_3 and Ni/γ-Al_2O_3 catalysts under various conditions in which 0.3 mol% CO was fed into the reactor with a lower space velocity. As shown in Fig. 7, both catalysts achieved high CO conversions over a wide reaction temperature range. In particular, the Ni/γ-Al_2O_3 catalyst achieved greater than 99% CO conversion at 210-250 °C.

CONCLUSIONS

CO and CO_2 methanation were investigated using Ni catalysts supported by alumina with different crystalline phases. Among these catalysts, Ni/θ-Al_2O_3 showed the highest activity for both CO and CO_2 methanation. The catalytic activity during CO methanation appears to be related to the number of Ni surface active sites, as determined by H_2-chemisorption. In the case of CO_2 methanation, Ni dispersion and the CO_2 adsorption site were found to be important factors in the catalytic activity. Ni/γ-Al_2O_3 and Ni/δ-Al_2O_3 are active in selective CO methanation in the presence of excess CO_2. The selective removal of CO can be achieved especially over Ni/γ-Al_2O_3 over a wide reaction temperature range.

ACKNOWLEDGEMENTS

This work was supported by the Human Resources Program in

Energy Technology (No. 20154010200820) of the Korea Institute of Energy Technology Evaluation and Planning (KETEP), which is granted financial resources from the Ministry of Trade, Industry and Energy of the Republic of Korea. This work was also supported by Basic Science Research Program through the National Research Foundation of Korea (NRF) funded by the Ministry of Science and ICT (2017R1A2B3011316).

SUPPORTING INFORMATION

Additional information as noted in the text. This information is available via the Internet at http://www.springer.com/chemistry/journal/11814.

REFERENCES

1. S. Rönsch, J. Schneider, S. Matthischke, M. Schlüter, M. Götz, J. Lefebvre, P. Prabhakaran and S. Bajohr, *Fuel*, **166**, 276 (2016).
2. M. Götz, J. Lefebvre, F. Mörs, A. M. Koch, F. Graf, S. Bajohr, R. Reimert and T. Kolb, *Renewable Energy*, **85**, 1371 (2016).
3. E. D. Park, D. Lee and H. C. Lee, *Catal. Today*, **139**, 280 (2009).
4. P. Sabatier and J. B. Senderens, *C.R. Acad. Sci. Paris*, **134**, 514 (1902).
5. B. Mao, S. S. K. Ma, X. Wang, H. Su and S. H. Chan, *Catal. Sci. Technol.*, **6**, 4048 (2016).
6. M. A. A. Aziz, A. A. Jalil, S. Triwahyono and A. Ahmad, *Green Chem.*, **17**, 2647 (2015).
7. J. Gao, Q. Liu, F. Gu, B. Liu, Z. Zhong and F. Su, *RSC Adv.*, **5**, 22759 (2015).
8. X. Su, J. Xu, B. Liang, H. Duan, B. Hou and Y. Huang, *J. Energy Chem.*, **25**, 553 (2016).
9. M. A. Vannice, *J. Catal.*, **37**, 449 (1975).
10. T. A. Le, M. S. Kim, S. H. Lee, T. W. Kim and E. D. Park, *Catal. Today*, **293-294**, 89 (2017).
11. S. Takenaka, T. Shimizu and K. Otsuka, *Int. J. Hydrogen Energy*, **29**, 1065 (2004).
12. M. Trueba and S. P. Trasatti, *Eur. J. Inorg. Chem.*, **17**, 3393 (2005).
13. I. Levin and D. Brandon, *J. Amer. Ceram. Soc.*, **81**, 1995 (1998).
14. E. V. Kul'ko, A. S. Ivanova, G. S. Litvak, G. N. Kryukova and S. V. Tsybulya, *Kinet. Catal.*, **45**, 714 (2004).
15. T. Sato, *Thermochim. Acta*, **88**, 69 (1985).
16. D. M. Sung, Y. H. Kim, E. D. Park and J. E. Yie, *Res. Chem. Intermed.*, **36**, 653 (2010).
17. E. V. Kul'ko, A. S. Ivanova, A. A. Budneva and E. A. Paukshtis, *Kinet. Catal.*, **46**, 132 (2005).
18. Y. H. Kim and E. D. Park, *Appl. Catal. B*, **96**, 41 (2010).
19. J. E. Park, B. B. Kim and E. D. Park, *Korean J. Chem. Eng.*, **32**, 2212 (2015).
20. J. H. Cho, S. H. An, T. S. Chang and C. H. Shin, *Catal. Lett.*, **146**, 811 (2016).
21. A. Patterson, *Phys. Rev.*, **56**, 978 (1939).
22. M. A. A. Aziz, A. A. Jalil, S. Triwahyono, R. R. Mukti, Y. H. Taufiq-Yap and M. R. Sazegar, *Appl. Catal. B*, **147**, 359 (2014).
23. C. Li and Y. W. Chen, *Thermochim. Acta*, **256**, 457 (1995).
24. J. Gao, C. Jia, J. Li, M. Zhang, F. Gu, G. Xu, Z. Zhong and F. Su, *J. Energ. Chem.*, **22**, 919 (2013).
25. S. Bali, J. Leisen, S. H. Foo, C. Sievers and C. W. Jones, *ChemSusChem*, **7**, 3145 (2014).
26. J. C. Lavalley, *Catal. Today*, **27**, 377 (1996).
27. Q. Pan, J. Peng, T. Sun, S. Wang and S. Wang, *Catal. Commun.*, **45**, 74 (2014).
28. J. Gao, C. Jia, M. Zhang, F. Gu, G. Xu and F. Su, *Catal. Sci. Technol.*, **3**, 2009 (2013).
29. P. Munnik, M. E. Z. Velthoen, P. E. Jongh, K. P. Jong and C. J. Gommes, *Angew. Chem. Int. Ed.*, **53**, 9493 (2014).
30. S. Bhatia, N. N. Bakhshi and J. F. Mathews, *Can. J. Chem. Eng.*, **56**, 575 (1978).
31. Y. Liu, J. Gao, Q. Liu, F. Gu, X. Lu, L. Jia, G. Xu, Z. Zhong and F. Su, *RSC Adv.*, **5**, 7539 (2015).
32. T. V. Herwijnen, H. V. Doesburg and W. A. D. Jong, *J. Catal.*, **28**, 391 (1973).
33. G. Garbarino, D. Bellotti, P. Riani, L. Magistri and G. Busca, *Int. J. Hydrogen Energy*, **40**, 9171 (2015).

Supporting Information

CO and CO_2 methanation over Ni catalysts supported on alumina with different crystalline phases

Thien An Le, Tae Wook Kim, Sae Ha Lee, and Eun Duck Park†

Department of Chemical Engineering and Department of Energy Systems Research, Ajou University, Suwon 16499, Korea
(*Received 8 August 2017 • accepted 18 September 2017*)

EXPERIMENTAL

1. Support Preparation

Bayerite was prepared using the precipitation method. The pH of the aqueous $Al(NO_3)_3 \cdot 9H_2O$ solution (Junsei Chem.) was increased to 10 by adding 1 M NH_4OH solution. The slurry was aged at room temperature for 10 days, filtered, and washed with distilled water. Then, the product was air dried at 110 °C for 1 day. η-Al_2O_3 and θ-Al_2O_3 were synthesized through the calcination of bayerite at 600 °C and 1,000 °C, respectively, for 4 h. κ-Al_2O_3 was obtained from gibbsite (Samchun Chem.) after calcination at 1,000 °C for 4 h. γ-Al_2O_3 and δ-Al_2O_3 were prepared through the calcination of boehmite (Aldrich) at 700 °C and 900 °C, respectively, for 4 h.

Table S1. Physical properties of alumina supports

Support	Surface area (m^2/g)	Pore volume (cm^3/g)	Average pore diameter[a] (nm)
θ-Al_2O_3	83	0.30	15
δ-Al_2O_3	81	0.26	13
η-Al_2O_3	184	0.27	6
γ-Al_2O_3	110	0.26	9
κ-Al_2O_3	14	0.15	43
α-Al_2O_3	<1	-	-

[a]Average pore diameter was determined using a BJH model

2. Catalyst Preparation

Ni/Al_2O_3 catalysts were prepared from an aqueous $Ni(NO_3)_2$ solution and alumina support using a wet impregnation method. Typically, 2.91 g of $Ni(NO_3)_2 \cdot 6H_2O$ (Junsei Chem.) was dissolved in 50 mL of deionized water; this solution was brought in contact with 5.3 g of Al_2O_3 at 60 °C for 6 h. Then, the excess water was slowly removed using a rotary evaporator (BUCHI, Switzerland). The recovered powder was dried in an oven at 120 °C for 12 h before calcination in an air stream at 500 °C for 3 h. The Ni content for all Ni/Al_2O_3 catalysts was intended to be 10 wt%.

3. Catalyst Characterization

The specific surface area of the catalysts was measured on a Micromeritics ASAP 2020 instrument and calculated using the Brunauer-Emmett-Teller (BET) method. Prior to measurement, the samples were degassed under vacuum for 6 h at 200 °C.

Powder X-ray diffraction (XRD) experiments were performed on a Rigaku D/Max instrument with a Cu Kα source. The primary crystallite sizes of the catalysts were determined using the Scherrer equation [1]:

$$L = \frac{0.9\lambda_{K\alpha 1}}{\beta_{(2\theta)}\cos\theta_{max}} \quad (1)$$

where L denotes the average particle size, 0.9 is the value in radi-

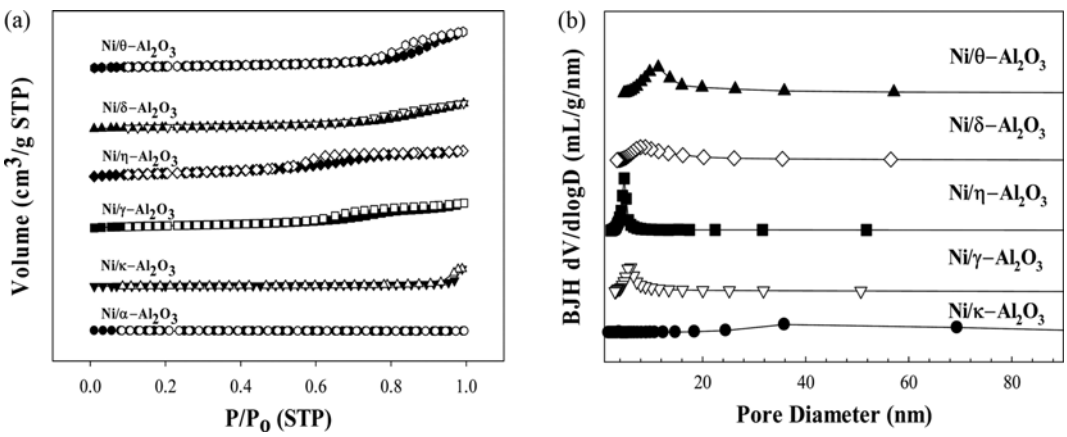

Fig. S1. (a) N_2 adsorption and desorption isotherms and (b) pore size distribution of Ni/Al_2O_3 catalysts with different alumina crystalline phases.

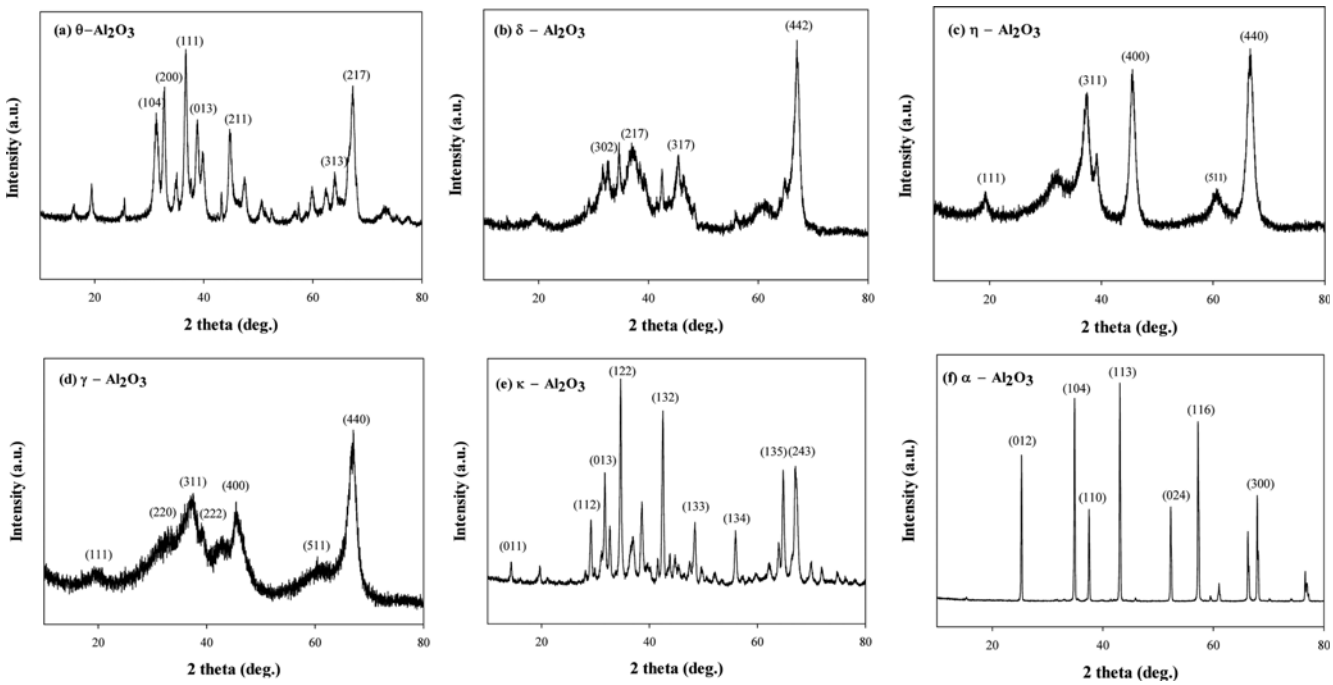

Fig. S2. X-ray diffraction patterns of alumina supports. (a) θ-Al_2O_3 (JCPDS 35-0121), (b) δ-Al_2O_3 (JCPDS 88-1609), (c) η-Al_2O_3 (JCPDS 04-0875), (d) γ-Al_2O_3 (JCPDS 29-0063), (e) κ-Al_2O_3 (JCPDS 88-0107), and (f) α-Al_2O_3 (JCPDS 42-1468).

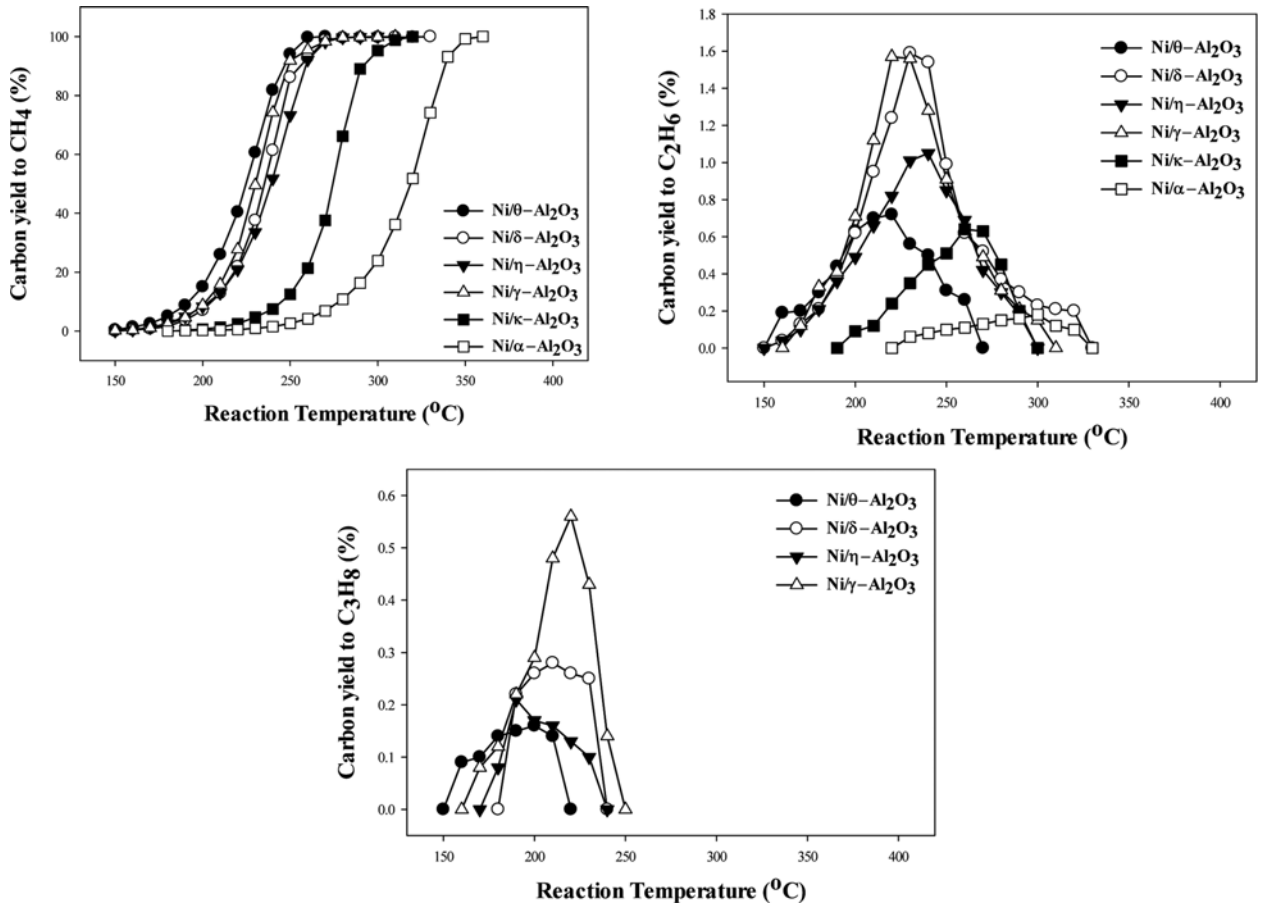

Fig. S3. Product yield for CO methanation over Ni/Al_2O_3 catalysts. Reaction conditions: 1 mol% CO, 50 mol% H_2, 49 mol% He, F/W=1,000 mL/min/g_{cat}.

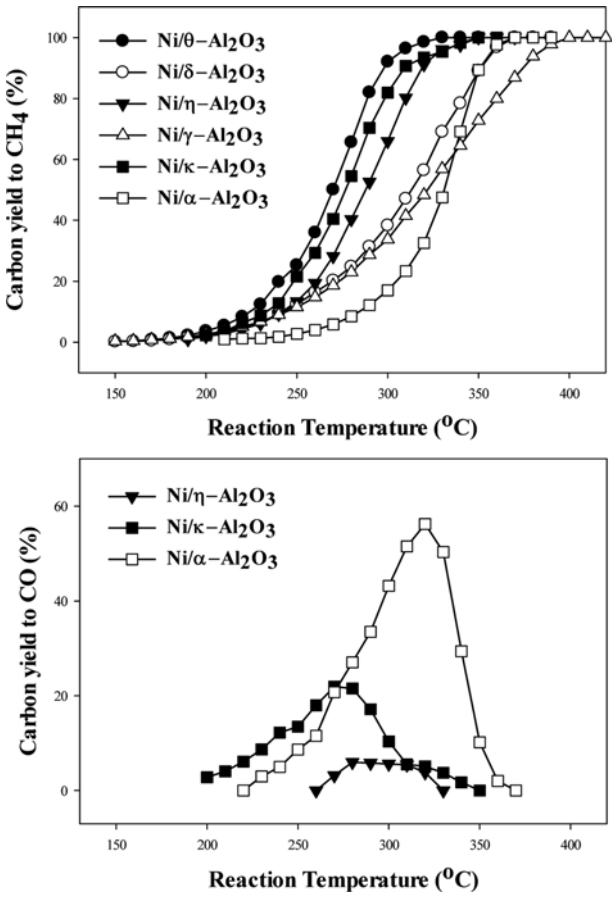

Fig. S4. Product yield for CO_2 methanation over Ni/Al_2O_3 catalysts. Reaction conditions: 1 mol% CO_2, 50 mol% H_2, 49 mol% He, F/W=1,000 mL/min/g_{cat}.

ans when $\beta_{(2\theta)}$ is the full width at half of the maximum peak height (FWHM), $\lambda_{K\alpha 1}$ is the wavelength of the X-ray radiation (0.15406 nm), and θ_{max} is the angular position of the (111) peak maximum of Ni.

Hydrogen temperature-programmed reduction (H_2-TPR) was performed on a Micromeritics 2910 Autochem equipped with a thermal conductivity detector (TCD). H_2-TPR was performed with 10 mol% H_2/Ar at a flow rate of 30 mL/min in the temperature range of 40-900 °C. The Ni content was established using the hydrogen consumption, which was calculated using the H_2-TPR patterns of predetermined amounts of Ag_2O. The degree of NiO reduction at 600 °C in each Ni/Al_2O_3 catalyst was calculated by comparing the amount of hydrogen consumed between 600 and 900 °C with the total amount of hydrogen consumed between 30 to 900 °C during the H_2-TPR experiment.

Pulsed CO_2 chemisorption and temperature-programmed desorption of CO_2 (CO_2-TPD) was performed on a Micromeritics Autochem 2910 to analyze the basic surface properties of the catalysts. Pulsed CO_2 chemisorption was conducted at room temperature via injection of 0.50 mL of 15 mol% CO_2 balanced with He into a He stream with a flow rate of 30 mL/min. CO_2-TPD was conducted in a He stream with a flow rate of 30 mL/min over a temperature range of 40-900 °C at a heating rate of 10 °C/min. The ion signals recorded at m/e=44 were used for monitoring desorbed CO_2.

The catalytic active surface area (CASA) of the catalyst was determined by H_2 chemisorption using a Micromeritics ASAP 2020. The catalyst was placed in a quartz sample cell and treated with a He flow (30 mL/min) at 100 °C for 1 h. The sample was evacuated and then purged in flowing H_2 for 5 min, and finally reduced under H_2 at 600 °C for 1 h at a heating rate of 10 °C/min. After reduction, the samples were evacuated for 1 h at 500 °C, followed by evacuation for 2 h at 35 °C. Before conducting further measurements, the samples were tested for any remaining H_2 leaks, followed by a final evacuation of 40 min at 35 °C. The double isotherm method was used to determine the amount of irreversibly chemisorbed H_2, which is calculated by extrapolating the linear part of the isotherm in the range of 95-450 mmHg to zero pressure; this value should correspond to the amount of H_2 adsorbed on the metallic Ni surface, considering the irreversible adsorption on the metallic Ni particle surface and reversible adsorption on the support surface. The Ni surface area can then be calculated under the assumptions that one hydrogen atom resides on one surface Ni atom and that the cross-sectional area of the Ni atom is 6.49×10^{-20} m^2 [2].

The metal content was confirmed using inductively coupled plasma-atomic emission spectroscopy (ICP-AES; Thermo Scientific iCAP 6500).

REFERENCES

1. A. Patterson, *Phys. Rev.*, **56**, 978 (1939).
2. M. A. A. Aziz, A. A. Jalil, S. Triwahyono, R. R. Mukti, Y. H. Taufiq-Yap and M. R. Sazegar, *Appl. Catal. B*, **147**, 359 (2014).